

The Boson peak in supercooled water

Pradeep Kumar

*Center for Studies in Physics and Biology, The Rockefeller University,
1230 York Avenue, New York, NY 10021 USA*

K. Thor Wikfeldt

*Science Institute and Faculty of Science, VR-III,
University of Iceland, 107 Reykjavík, ICELAND and
Nordita, Royal Institute of Technology and Stockholm University,
Roslagstullsbacken 23, S-10691 Stockholm, SWEDEN*

Daniel Schlesinger and Lars G. M. Pettersson

Department of Physics, AlbaNova, Stockholm University, S-10691 Stockholm, SWEDEN

H. Eugene Stanley

*Center for Polymer Studies and Department of Physics,
Boston University, Boston, MA 02215 USA*

Abstract

We perform extensive molecular dynamics simulations of the TIP4P/2005 model of water to investigate the origin of the Boson peak reported in experiments on supercooled water in nanoconfined pores, and in hydration water around proteins. We find that the onset of the Boson peak in supercooled bulk water coincides with the crossover to a predominantly low-density-like liquid below the Widom line T_W . The frequency and onset temperature of the Boson peak in our simulations of bulk water agree well with the results from experiments on nanoconfined water. Our results suggest that the Boson peak in water is not an exclusive effect of confinement. We further find that, similar to other glass-forming liquids, the vibrational modes corresponding to the Boson peak are spatially extended and are related to transverse phonons found in the parent crystal, here ice Ih.

Introduction:

One of the characteristic features of many glasses and amorphous materials is the onset[1] of low-frequency collective modes (Boson peak) in the energy range $2 - 10$ meV at low T , where the vibrational density of states (VDOS) $g(\omega)$ shows an excess over $g(\omega) \propto \omega^2$ predicted by the Debye model. Disordered materials are further known to exhibit many anomalous behaviors compared to their crystalline counterparts, such as the temperature dependence of thermal conductivity[2, 3] and specific heat[4, 5] at low temperatures. Many scenarios[6, 7] have been suggested to explain the physical mechanisms behind the Boson peak and related anomalies, but a comprehensive understanding has proved elusive.

Recent neutron scattering experiments on water confined in nanopores indicate the presence of a Boson peak[8, 9] around $5 - 6$ meV ($40 - 49$ cm $^{-1}$) emerging below 230 K in the incoherent dynamic structure factor. These results were tentatively interpreted as arising from a gradual change in the local structure of confined liquid water when crossing the Widom line temperature T_W [10]. Earlier, neutron scattering has also been applied to protein hydration water [11] and a Boson peak was found around 30 cm $^{-1}$. T_W corresponds to the loci of maxima of thermodynamic response functions in the one-phase region beyond the liquid-liquid critical point (LLCP) proposed to exist in supercooled liquid water[12]. A Widom line in the supercritical region in argon has recently been studied[13, 14] and found to be directly related to a dynamical crossover between liquid-like and gas-like properties, but the existence of a dynamical crossover in supercooled water is subject to some controversy [15–23]. Since the melting temperature is strongly depressed in nanoconfinement and in protein hydration water, deeply supercooled confined water has been used experimentally to infer the behavior of bulk water, which is more challenging to supercool. However, the similarity to bulk water has been called into question[24, 25], and it is thus important to further investigate the relationship between water in these different forms.

Both experimental[9, 26] and simulation[27] studies suggest that the density relaxation of confined and hydration water at and slightly below the Widom temperature is of the order of a few tens of nanoseconds, implying that liquid water is still in metastable equilibrium over the experimental time scales involved[28]. The experimental observation of a Boson peak below T_W in confined water thus suggests that the low-density-like liquid shares vibrational properties with the glassy state, as has been observed previously for other systems such as

B_2O_3 [29, 30]. On the other hand, the dynamic structure factor of crystalline ice exhibits a peak at a slightly higher frequency around 50 cm^{-1} [31–33] as do the Raman spectra of ice Ih and proton-ordered ice XI[34]; in the latter case the peak becomes extremely sharp. These results indicate a connection between the dynamics of supercooled liquid and crystalline vibrational dynamics. Indeed, it has recently been suggested that Boson peaks observed in glasses are related to the vibrational dynamics of the parent crystal[35].

To shed light on the question of whether bulk supercooled liquid water displays a Boson peak, we study the low-frequency dynamics of the TIP4P/2005 model of water which accurately reproduces a range of water properties [36], including its anomalies [37]. This model has been found to exhibit a LLCPP in the vicinity of $P_C = 1350 \text{ bar}$ and $T_C = 193 \text{ K}$ [38]. The associated Widom line has been shown to be accompanied by a structural crossover from a predominantly high-density liquid (HDL) structure to a predominantly low-density liquid (LDL) structure[39, 40] occurring at a temperature T_W around 230 K at 1 bar . We find that this water model indeed displays a Boson peak in the bulk supercooled regime and that its onset coincides with the Widom temperature. Our analysis further shows that it derives from transverse acoustic modes in the parent crystal, ice Ih, in agreement with the recently proposed picture[35]. We further verify our results using another model of water, TIP5P, and find also in this case an emergence of a Boson peak below the Widom line.

Results

A. Incoherent dynamic structure factors:

A quantity that is readily accessible in inelastic neutron scattering experiments is the incoherent dynamic structure factor (DSF) $S_S(k, \omega)$ which probes single-particle dynamics. To compare our simulation results with experiment we first calculate the self-intermediate scattering function

$$F_S(k, t) = \left\langle \frac{1}{N} \sum_i e^{i\mathbf{k} \cdot [\mathbf{r}_i(t) - \mathbf{r}_i(0)]} \right\rangle \quad (1)$$

where $\mathbf{r}_i(t)$ are the positions of oxygen atoms, N is the number of molecules and angular brackets denote an ensemble average and averaging over different \mathbf{k} with the same modulus. In simulations the wave vector \mathbf{k} is defined as $\frac{2\pi}{L}(n_x, n_y, n_z)$ for integers (n_x, n_y, n_z) and system size L . We perform the frequency decomposition of $F_S(k, t)$ to obtain the incoherent

DSF

$$S_S(k, \omega) \equiv \int F_S(k, t) e^{i\omega t} dt. \quad (2)$$

In Figs. 1(a) and 1(b), we show $F_S(k, t)$ and $S_S(k, \omega)$ for supercooled liquid water simulations with $N = 512$ molecules at atmospheric pressure and different temperatures for $k = 2 \text{ \AA}^{-1}$, *i.e.*, the position of the first peak in the structure factor $S(k)$. For $T < T_W$, a minimum appears in $F_S(k, t)$ around 0.3 ps followed by oscillations up to around 10 ps. In the incoherent DSF these changes with temperature correspond to the emergence of sharp peaks at 20 and 25 cm^{-1} along with a broad peak centered around 37 cm^{-1} . For comparison, we also show $F_S(k, t)$ and $S_S(k, \omega)$ from hexagonal ice simulations at 100 K for two different system sizes. The connection between liquid and crystalline low-frequency dynamics will be further discussed below but we note here that the system size obviously affects the region $\omega < 40 \text{ cm}^{-1}$.

Since low-frequency dynamics in supercooled liquids and glasses may be affected by finite-size effects [41–43], we show in Figs. 1(c) and 1(d) a comparison with a much larger system, $N = 45,000$ at 210 K. In $F_S(k, t)$ the oscillations are shifted to longer times while the minimum at 0.3 – 0.4 ps and subsequent peak around 0.9 ps are system-size independent. The sharp peaks in $S_S(k, \omega)$ vanish in the large simulation but the broad peak around 37 cm^{-1} persists; we therefore label this peak of low-frequency excitations as the Boson peak. Comparing our simulation results with experimental neutron data on protein hydration water[11] and on water in confinement[8, 9] reveals rather good agreement. Both the experimental energy position, 30 cm^{-1} for hydration water[11] and 45 cm^{-1} for confined water[8, 9], and the temperature onset, $T = 225 \text{ K}$ [8, 9], are surprisingly well reproduced by the TIP4P/2005 model considering the approximate nature of classical force fields. Since we observe well-defined low-frequency modes in the incoherent DSF in the simulations of bulk water, we conclude that the Boson peak in supercooled water is not a consequence of confinement and that it would likely be detected also in experiments on bulk water, if sufficient supercooling could be achieved.

A connection to the Widom line in TIP4P/2005 is clearly present since a qualitative change of both $F_S(k, t)$ and $S_S(k, \omega)$ takes place between 230 and 240 K. Our results thus imply that a Boson peak may also appear in other tetrahedral [44] liquids, such as silicon and silica, for which simulations have indicated the existence of a liquid-liquid phase transition[45, 46]. To confirm the connection between the Boson peak and the Widom line we

have performed additional simulations of a different water potential, the TIP5P model[47], which has been shown to exhibit a Widom line around 250 K[27], 20 K above that for TIP4P/2005. As shown in the Supplementary Information, a Boson peak emerges also in this model and, indeed, it coincides with T_W at 250 K.

B. Vibrational density of states:

The Boson peak is commonly discussed in terms of the VDOS, $g(\omega)$. A distinct peak is often not seen in the VDOS itself but appears only in the reduced VDOS after normalizing by the squared frequency, $g(\omega)/\omega^2$, which reveals the excess over the Debye model prediction $g(\omega) \propto \omega^2$. We calculate $g(\omega)$ as the Fourier transform of the oxygen velocity autocorrelation function, $C_v(t)$:

$$g(\omega) \equiv \int C_v(t) e^{i\omega t} dt, \quad (3)$$

where

$$C_v(t) = \left\langle \frac{1}{N} \sum_i \vec{v}_i(t) \vec{v}_i(0) \right\rangle. \quad (4)$$

The sum includes all N oxygens in the system, \vec{v}_i are the oxygen atom velocities and $\langle \dots \rangle$ denotes the ensemble average.

In Fig. 2(a) we show graphs of $g(\omega)$ for various temperatures. Below T_W , $g(\omega)$ shows an onset of the same two sharp low-frequency peaks as observed in $S_S(k, \omega)$ in Fig. 1. By simulating a range of different system sizes we can establish the system-size dependence of $g(\omega)$. The agreement for frequencies $\omega > 40 \text{ cm}^{-1}$ is very good for different system sizes L , but the sharp low-frequency peaks shift to lower frequencies as the system size is increased. Indeed, both peaks extrapolate linearly to zero as $1/L$, as seen in the inset of Fig. 2(a), suggesting that they disappear in the limit of infinite system size.

As discussed in relation to Fig. 1, there is a low-frequency peak in $S_S(k, \omega)$ for hexagonal ice at somewhat higher frequency compared to the supercooled liquid simulations, suggesting a link between the liquid and crystalline low-frequency modes. We investigate this by performing thermally non-equilibrated simulations at even lower temperatures where the TIP4P/2005 model vitrifies to a low-density amorphous (LDA)-like solid. The non-equilibrium simulations are performed by annealing the equilibrated metastable 210 K simulation with a cooling rate of $2 \cdot 10^{10} \text{ K/s}$ to reach target temperatures of 150 and 100 K.

Figure 2(b) shows the reduced VDOS, $[g(\omega) - g(0)]/\omega^2$ for simulations at 100, 150 and 210 K compared to the hexagonal ice simulation at 100 K. We subtract an extrapolated value of $g(0)$ from $g(\omega)$ to eliminate uncertainties due to the finite length of the trajectories when evaluating the Fourier transform in Eq. (3). A clear shift to higher frequencies of the Boson peak is observed as the supercooled liquid simulations are cooled into the LDA glass region, and the reduced VDOS at 100 K resembles the crystalline ice counterpart.

In the inset of Fig. 2(b), we show the reduced VDOS $g_{NM}(\omega)/\omega^2$ obtained from the normal modes of the liquid calculated from quenched configurations (*i.e.*, energy minimized inherent structures) at $T = 210$ K. We find that the Boson peak in $g_{NM}(\omega)/\omega^2$ is blue-shifted to around 50 cm^{-1} , close to the peak for hexagonal ice, compared to the velocity autocorrelation function VDOS which peaks at 37 cm^{-1} . This suggests that a key difference in low-frequency vibrational properties between the LDL-like liquid below the Widom line and crystalline ice lies in the more anharmonic dynamics of the liquid phase.

C. Transverse and longitudinal correlation functions:

Having established the existence of a Boson peak in supercooled water below the Widom line and its connection to low-frequency dynamics present in the parent crystal, ice Ih, we now turn to the study of transverse and longitudinal current correlations to clarify the nature of these low-frequency modes. We calculate longitudinal and transverse currents as

$$J_L(\mathbf{k}, t) = \sum_{i=1}^N \hat{\mathbf{k}}_{\parallel} \cdot \mathbf{v}_i(t) \exp[-i\mathbf{k} \cdot \mathbf{r}_i(t)] , \quad (5)$$

$$J_T(\mathbf{k}, t) = \sum_{i=1}^N \hat{\mathbf{k}}_{\perp} \cdot \mathbf{v}_i(t) \exp[-i\mathbf{k} \cdot \mathbf{r}_i(t)] \quad (6)$$

where $\hat{\mathbf{k}}_{\parallel}$ and $\hat{\mathbf{k}}_{\perp}$ are unit vectors respectively parallel and perpendicular to \mathbf{k} , and $\mathbf{r}_i(t)$ and $\mathbf{v}_i(t)$ denote the oxygen atoms' position and velocity, respectively. The frequency decomposition of the longitudinal and transverse current autocorrelation functions is

$$C_{\alpha}(k, \omega) \equiv \int \langle J_{\alpha}(k, t) J_{\alpha}(-k, 0) \rangle e^{i\omega t} dt \quad (7)$$

where $\alpha = L$ or T .

In the bottom part of Fig. 2(a) we show superimposed on the VDOS the transverse current correlation function (TCCF) $C_T(k, \omega)$ at different temperatures for the lowest wave number

k accessible in the $N=512$ simulation boxes, *i.e.*, $\mathbf{k} = 2\pi(1,0,0)/L$ and permutations thereof. We see that the first sharp size-dependent low-frequency peak in VDOS, which develops below T_W , coincides exactly with the lowest- k TCCF, and the second finite-size peak around 25 cm^{-1} coincides with the second-lowest- k TCCF (not shown). Returning to Fig. 1(d), the low-frequency side of the Boson peak is smoother in the large $N = 45,000$ simulations and the sharp peaks related to the lowest- k transverse currents are instead seen at frequencies below 10 cm^{-1} . We thus conclude that the sharp system size dependent low-frequency peaks around the Boson peak frequency and below are predominantly transverse excitations, consistent with previous findings for amorphous silica [43].

The dispersion relations for transverse and longitudinal current spectra, $C_T(k, \omega)$ and $C_L(k, \omega)$ at $T = 210 \text{ K}$, and $P = 1 \text{ atm}$ are shown in Fig. 3 (the current spectra are shown in the Supplementary Material). We obtain dispersion relations by fitting damped harmonic oscillator (DHO) [48] lines to both longitudinal and transverse spectra.

At small k below 0.5 \AA^{-1} , the longitudinal current spectrum, $C_L(k, \omega)$, shows only one acoustic dispersing excitation. For $k > 0.5 \text{ \AA}^{-1}$, $C_L(k, \omega)$ shows the existence of three excitations and can be fit with three DHO lines. Besides the dispersing excitation at intermediate frequency, two other nondispersing excitations appear—one at low frequency around 50 cm^{-1} and the other at high frequency around 260 cm^{-1} . The intensity of these excitations in $C_L(k, \omega)$ increases upon further increase of k . Transverse current spectra $C_T(k, \omega)$ exhibit an acoustic dispersing excitation $k < 0.5 \text{ \AA}^{-1}$. For $k > 0.5 \text{ \AA}^{-1}$, $C_T(k, \omega)$ develops a peak at $\omega \approx 260 \text{ cm}^{-1}$, the same excitation as in the longitudinal current spectra. Transverse and longitudinal modes are thus strongly mixed above 0.5 \AA^{-1} as has been found previously also for the SPC/E water model [49]. Moreover, the mixing happens at both high frequencies ($\omega \approx 260 \text{ cm}^{-1}$) and low frequencies ($\omega < 60 \text{ cm}^{-1}$) as evident from transverse excitations appearing in longitudinal spectra. We note that the band at 260 cm^{-1} in liquid water is associated with four-coordinated water molecules since low-frequency Raman spectra of water down to -20° C showed its intensity to increase with decreasing temperature [50] and hexagonal ice also displays a strong band near this frequency [51]. Hence, the emergence of the 260 cm^{-1} band in both $C_L(k, \omega)$ and $C_T(k, \omega)$ suggests that liquid water at this temperature exhibits networks of four-coordinated molecules over length scales as large as $2\pi/0.5 \text{ \AA}^{-1} \sim 13 \text{ \AA}$. This observation is also consistent with recent studies where it is shown that the sizes of clusters of highly tetrahedral molecules increases below the Widom

temperature[3, 44].

The emergence of an additional, high-frequency excitation in $C_L(k, \omega)$ and $C_T(k, \omega)$ around 260 cm^{-1} for $k > 0.5 \text{ \AA}^{-1}$ suggests a low-frequency liquid-like and a high-frequency solid-like response of the longitudinal and transverse spectra at this length scale and a concomitant pile-up of spectral intensity takes place in the Boson peak regime.

To get further insights into the longitudinal or transverse character of the Boson peak, we compare cumulatively integrated spectra over k for different frequencies for both the transverse and longitudinal parts, $C_L^*(k, \omega)$ and $C_T^*(k, \omega)$, defined as

$$C_\alpha^*(k, \omega) = \int_{k_{\min}}^k C_\alpha(k', \omega) dk', \quad (8)$$

where $\alpha = L$ or T and $k_{\min} = 2\pi/L$ is the smallest wave number accessible in our system of box size L . $C_\alpha^*(k, \omega)$ thus describes the total contribution of longitudinal and transverse modes with different wave numbers up to k for a given frequency ω . In Fig. 4(a)-(b) we show $C_L^*(k, \omega_B)$ and $C_T^*(k, \omega_B)$ for several frequencies ω_B in the Boson peak region around 37 cm^{-1} . It can be clearly seen that transverse modes are dominant in the Boson peak frequency regime for $k > 0.5 \text{ \AA}^{-1}$.

D. Localization analysis:

A number of studies on amorphous materials have found that the modes in the Boson peak frequency range are localized or quasi-localized[52, 53]. In order to investigate whether this holds also for TIP4P/2005 water below the Widom line T_W we calculate the degree of localization by performing a normal mode analysis of quenched (or inherent) structures, obtained by energy-minimizing snapshots from simulation trajectories. A measure of the degree of localization of a vibrational mode is the frequency-dependent participation ratio[54, 55] p_μ for mode μ

$$p_\mu = \left[N \sum_{i=1}^N (u_\mu^i \cdot u_\mu^i)^2 \right]^{-1} \quad (9)$$

where u_μ^i is the contribution of all degrees of freedom of molecule i to the normal mode μ . The participation ratio is unity when all molecules contribute equally to the normal mode in consideration, while $p = 1/N$ if only one molecule contributes to the total energy of the mode. Hence, for an extended mode p_μ is quite large and does not depend on the system size while for a localized mode it is small and scales with system size as $1/N$. One way

to determine the extent of localization is thus to inspect the system-size dependence of the participation ratio. We find (see Fig. 5(a)) that the participation ratio is quite large, around 0.6, for the modes with frequency below 50 cm^{-1} , the region of the Boson peak. Apart from the sharp finite-size peaks, the participation ratio for the modes in the region of the Boson peak show only a weak system size dependence, suggesting that the modes giving rise to the Boson peak are not localized but extended.

We next introduce a function $A_{\text{max}}(r)$ defined as the maximum displacement of molecules at a distance r from the molecule with the largest displacement in the normal mode. For a localized mode a rapid decay of $A_{\text{max}}(r)$ should be seen. In Fig. 5(b) we show average $A_{\text{max}}(r)$ for the normal modes in two different frequency regimes – for the Boson peak regime ($\omega_B = 45 \pm 2.5 \text{ cm}^{-1}$, note that the frequency of the Boson peak for the quenched configuration is shifted to higher frequency compared to the Boson peak frequency $\omega_B \approx 37 \text{ cm}^{-1}$ of the liquid at $T = 210 \text{ K}$, see inset of fig. 2(b)), and in comparison we also show average $A_{\text{max}}(r)$ for modes in the range of $\omega = 400 \pm 5 \text{ cm}^{-1}$, which is a range of localized vibrations. While for $\omega = 400 \pm 5 \text{ cm}^{-1}$, $A_{\text{max}}(r)$ decays rapidly to zero, for the Boson peak region it does not, suggesting again an extended nature of the Boson peak modes.

Discussion

The low-frequency vibrations of a classical potential model of water, TIP4P/2005, are investigated in the supercooled temperature regime to clarify the origin of the Boson peak reported from inelastic neutron scattering experiments below around 225 K in nano-confined[8, 9] and protein-hydration water[11]. We find that sharp low-frequency peaks emerge in the incoherent dynamic structure factor and the reduced density of states of the simulated liquid water as the system is cooled below the Widom line, but a system-size investigation reveals that in the limit of an infinitely large simulation box these peaks extrapolate to zero frequency. The sharp finite-size peaks are seen to coincide exactly with the inherently discrete, low wave-number acoustic branch of the transverse current correlation functions, reflecting a strong contribution of transverse modes in this frequency region. However, we find a broad Boson peak centered around 37 cm^{-1} which is unaffected by system size, and for which the frequency region and temperature onset in the incoherent DSF agree well with neutron experiments on confined water. Due to its lower melting temperature, water

in confinement has been used experimentally to infer the behavior of bulk water below the bulk homogeneous nucleation temperature. The validity of this comparison has been questioned, but the good agreement observed here in the low-frequency vibrational dynamics lends support to the view of confinement as useful in the study of supercooled bulk water, at least for low-frequency vibrational properties.

The frequency of the Boson peak in supercooled TIP4P/2005 water as observed in the reduced VDOS changes as the simulation is annealed into the LDA glass region and approaches $\omega = 45 \text{ cm}^{-1}$. This is also the frequency at which hexagonal ice simulations display a peak in vibrational spectra deriving from the transverse acoustic branch, as has been observed experimentally[31–33]. Thus, upon lowering the temperature below the Widom line, the low-frequency dynamics of the system progressively changes from LDL-like to LDA glass and to the dynamics found in hexagonal ice. A similar shift to higher frequencies is observed in normal-mode spectra of inherent structures quenched from liquid at temperatures below the Widom line, indicating that the lower frequency of the Boson peak in the liquid below the Widom line, compared to the transverse acoustic peak in the ice, is a result of the more anharmonic nature of the vibrational modes in the liquid.

Recent work by Chumakov *et al.*[35] on glasses suggests that there is no excess in the actual number of states at the Boson peak and hence no additional modes compared to the crystal. The Boson peak is thus related to the transverse acoustic singularity of the underlying crystal structure. Transverse modes have also been firmly connected to the Boson peak in other works [43, 56]. Indeed, our studies of transverse and longitudinal correlation functions suggest that low-frequency transverse phonons contribute the most to the Boson peak intensity in the range of wave numbers where both the longitudinal and transverse phonons show a solid-like response over large length scales, namely emergence of a high-frequency peak in both longitudinal and transverse spectra at $\omega \approx 260 \text{ cm}^{-1}$ for $k > 0.5 \text{ \AA}^{-1}$. The appearance of this high-frequency excitation associated with four-coordinated molecules in longitudinal and transverse spectra coincides with a pile up of intensities in the Boson peak regime.

To conclude, our results indicate that liquid water displays a Boson peak below the Widom line temperature T_W . Both the onset temperature and energy position are similar to what has been observed experimentally for confined water [8, 9]. We find that as the liquid crosses over to a low-density-like liquid structure below T_W the low-frequency dynamics of

the liquid changes to resemble that of the underlying crystal, ice Ih. The Boson peak in supercooled water is thus a manifestation of the transverse acoustic singularity of the crystal and may therefore be a general phenomenon in tetrahedral liquids showing a liquid-liquid phase transition.

Methods

We simulate TIP4P/2005[36] water for a range of temperatures at atmospheric pressure. Equilibration is first performed in the NPT ensemble, using the Nosé-Hoover thermostat and Parrinello-Rahman barostat to attain constant temperature and pressure. The equilibrated densities are then used in equilibration NVT runs performed over multiple structural relaxation times, after which we switch to the NVE ensemble to compute the relevant dynamical quantities. The equations of motion are integrated with a time step of 0.2-1.0 fs, depending on the observed energy conservation. Most simulations are performed using $N=512$ molecules, but to quantify the finite-size effects we simulate larger systems up to $N=45,000$. Simulation temperatures between 210 and 260 K at $P = 1$ atm were chosen so that the system crosses T_W , the temperature where maxima in response functions are observed. To confirm the connection between the Widom line T_W and the onset temperature of the Boson peak we repeat the above simulation protocol for the TIP5P water model[47] at temperatures between 240 and 270 K (see Supplementary Information).

We perform non-equilibrium simulations of TIP4P/2005 at 100 and 150 K by rapidly cooling from 210 K with a cooling rate of $2 \cdot 10^{10}$ K/s, and then switching to the NVE ensemble to calculate dynamical properties.

For the calculation of the participation ratio and the function $A_{\max}(r)$, equilibrium configurations at a given temperature were quenched to obtain the configurations corresponding to the nearest local minimum of the system. Then we calculate eigenmodes and eigenvalues corresponding to vibrational modes about this local energy minimum by diagonalizing the Hessian matrix with respect to the generalized coordinates. We use the flexible version of the model and hence all degrees of freedom to calculate the Hessian (see Refs. [54, 55, 57]

for a more detailed explanation of the formalism and method).

- [1] Angell, C. A. Boson peaks and floppy modes: some relations between constraint and excitation phenomenology, and interpretation, of glasses and the glass transition. *J. Phys.: Condens. Matter*, 16:S5153, 2004.
- [2] Cahill, D. G. & Pohl, R. O. Lower limit to the thermal conductivity of disordered crystals. *Phys. Rev. B*, 35:4067, 1987.
- [3] Kumar, P. & Stanley H. E. Thermal conductivity minimum: A new water anomaly. *J. Phys. Chem. B*, 115:14269–14273, 2011.
- [4] Berman, R. Thermal conductivity of glasses at low temperatures. *Phys. Rev.*, 76:315–316, 1949.
- [5] Zeller, R. C. & Pohl, R. O. Thermal conductivity and specific heat of noncrystalline solids. *Phys. Rev. B*, (4):2029, 1971.
- [6] Nakayama, T. Boson peak and terahertz frequency dynamics of vitreous silica. *Rep. Prog. Phys.*, 65:1195, 2002.
- [7] Angell, C. A., Ngai, K. L., McKenna, G. B., McMillan, P. F. & Martin, S. W. Relaxation in glassforming liquids and amorphous solids. *J. Appl. Phys.*, 88:3113–3147, 2000.
- [8] Chen, S. -H. et. al. Dynamic crossover phenomenon in confined supercooled water and its relation to the existence of a liquid-liquid critical point in water. In *AIP Conference Proceedings*, volume 982:39–52, 2008.
- [9] Chen, S. -H. et. al. Evidence of dynamic crossover phenomena in water and other glass-forming liquids: experiments, MD simulations and theory. *J. Phys.: Condens. Matter*, 21:504102, 2009.
- [10] Kumar, P. et. al., Glass transition in biomolecules and the liquid-liquid critical point of water. *Phys Rev Lett*, 97:177802, 2006.
- [11] Paciaroni, A., Bizzarri, A. R. & Cannistaro, S. Neutron scattering evidence of a boson peak in protein hydration water. *Phys. Rev. E*, 60:2476–2479, 1999.
- [12] Poole, P. H., Sciortino, F., Essmann U. & Stanley H. E.. Phase behaviour of metastable water. *Nature*, 360(6402):324–328, 1992.
- [13] Simeoni, G. et. al. The Widom line as the crossover between liquid-like and gas-like behaviour in supercritical fluids. *Nature Physics*, 6:503–507, 2010.

- [14] Gorelli, F. A. et. al. Dynamics and thermodynamics beyond the critical point. *Sci. Rep.*, 3:1203, 2013.
- [15] Faraone, A., Liu, L., Mou, C.-Y., Yen, C.-W. & Chen, S.-H. Fragile-to-strong liquid transition in deeply supercooled confined water. *J. Chem. Phys.*, 121:10843, 2004.
- [16] Mamontov, E. Observation of fragile-to-strong liquid transition in surface water in CeO_2 . *J. Chem. Phys.*, 123:171101, 2005.
- [17] Swenson, J., Jansson, H. & Bergman, R. Relaxation processes in supercooled confined water and implications for protein dynamics. *Phys. Rev. Lett.*, 96:247802, 2006.
- [18] Mallamace, F. et. al. The fragile-to-strong dynamic crossover transition in confined water: nuclear magnetic resonance results. *J. Chem. Phys.*, 124:161102, 2006.
- [19] Swenson, J., Jansson, H., Hedström, J. & Bergman, R. Properties of hydration water and its role in protein dynamics. *J. Phys.: Cond. Matt.*, 19:205109, 2007.
- [20] Khodadadi, S. et. al. The origin of the dynamic transition in proteins. *J. Chem. Phys.*, 128:195106, 2008.
- [21] Pawlus, S., Khodadadi, S. & Sokolov, A. P. Conductivity in hydrated proteins: no signs of the fragile-to-strong crossover. *Phys. Rev. Lett.*, 100:108103, 2008.
- [22] Vogel, M. Origins of apparent fragile-to-strong transitions of protein hydration waters. *Phys. Rev. Lett.*, 101:225701, 2008.
- [23] Vogel, M. Temperature-dependent mechanisms for the dynamics of protein-hydration waters: a molecular dynamics simulation study. *J. Phys. Chem. B*, 113:9386–9392, 2009.
- [24] Ricci, M. A., Bruni, F., Gallo, P., Rovere, M. & Soper, A. K. Water in confined geometries: experiments and simulations. *J. Phys.: Condens. Matter*, 12:A345, 2000.
- [25] Mattea, C., Qvist, J. & Halle, B. Dynamics at the protein-water interface from ^{17}O spin relaxation in deeply supercooled solutions. *Biophys. J.*, 95:2951–2963, 2008.
- [26] Chen, S. -H. et. al. Observation of fragile-to-strong dynamic crossover in protein hydration water. *Proc Natl Acad Sci (USA)*, 103:9012–9016, 2006.
- [27] Xu, L. et. al. Relation between the Widom line and the dynamic crossover in systems with a liquid–liquid phase transition. *Proc. Natl. Acad. Sci. USA*, 102:16558–16562, 2005.
- [28] Liu, L., Chen, S.-H., Faraone, A., Yen, C.-W. & Mou, C.- Y. Pressure dependence of fragile-to-strong transition and a possible second critical point in supercooled confined water. *Phys. Rev. Lett.*, 95:117802, 2005.

- [29] Börjesson, L., Hassan, A. K., Swenson, J, Torell, L. M. & A. Fontana. Is there a correlation between the first sharp diffraction peak and the low frequency vibrational behavior of glasses? *Phys. Rev. Lett.*, 70:1275–1278, 1993.
- [30] Sokolov, A. P., Kisliuk, A., Quitmann, D., Kudlik, A. & Rössler, E. The dynamics of strong and fragile glass formers: vibrational and relaxation contributions. *J. Non-Cryst. Sol.*, 172:138–153, 1994.
- [31] Bermejo, F. J., Alvarez, M., Bennington, S. M. & Vallauri, R. Absence of anomalous dispersion features in the inelastic neutron scattering spectra of water at both sides of the melting transition. *Phys. Rev. E*, 51:2250, 1995.
- [32] Yamamuro, O. et. al Low-energy excitations of vapor-deposited amorphous ice and its annealing and methanol-doping effects studied by inelastic neutron scattering. *J. Chem. Phys.*, 115:9808, 2001.
- [33] Yamamuro, O., Matsuo, T., Tsukushi, I, & Onoda-Yamamuro, N. Inelastic neutron scattering and low-energy excitation of amorphous SF₆ hydrate prepared by vapor-deposition technique. *Can. J. Phys.*, 81:107–114, 2003.
- [34] Abbe, K. & Shigenari, T. Raman spectra of proton ordered phase XI of ice I. Translational vibrations below 350 cm⁻¹. *J. Chem. Phys.*, 134:10506, 2011.
- [35] Chumakov, A.I. et. al. Equivalence of the Boson peak in glasses to the transverse acoustic van Hove singularity in crystals. *Phys. Rev. Lett.*, 106:225501–225504, 2011.
- [36] Abascal, J. L. F. & Vega, C. A general purpose model for the condensed phases of water: TIP4P/2005. *J. Chem. Phys.*, 123:234505, 2005.
- [37] Pi, H. L. et. al. Anomalies in water as obtained from computer simulations of the TIP4P/2005 model: density maxima, and density, isothermal compressibility and heat capacity minima. *Mol Phys*, 107:365–374, 2009.
- [38] Abascal, J. L.F. & Vega, C. Widom line and the liquid–liquid critical point for the TIP4P/2005 water model. *J. Chem. Phys.*, 133:234502, 2010.
- [39] Wikfeldt, K. T., Huang, C., Nilsson, A. & Pettersson, L. G. M. Enhanced small-angle scattering connected to the Widom line in simulations of supercooled water. *J. Chem. Phys.*, 134:214506–214516, 2011.
- [40] Wikfeldt, K. T., Nilsson, A. & Pettersson, L.G.M. Spatially inhomogeneous bimodal inherent structure in simulated liquid water. *Phys. Chem. Chem. Phys.*, 13:19918–19924, 2011.

- [41] Horbach, J., Kob, W., Binder, K. & Angell, C. A. Finite size effects in simulations of glass dynamics. *Phys. Rev. E*, 54:5897–5900, 1996.
- [42] Kim, K. & Yamamoto, R. Apparent finite-size effects in the dynamics of supercooled liquids. *Phys. Rev. E*, 61:41–44, 2000.
- [43] Horbach, J., Kob, W. & Binder, K. High frequency sound and the boson peak in amorphous silica. *Eur Phys J B*, 19:531–543, 2001.
- [44] Errington, J. R. & Debenedetti, P. G. Relationship between structural order and the anomalies of liquid water. *Nature*, 409:318–321, 2001.
- [45] Sastry, S. & Angell, C. A. Liquid–liquid phase transition in supercooled silicon. *Nature Mat*, 2:739–743, 2003.
- [46] Saika-Voivoid, I., Sciortino, F. & Poole, P. H. Computer simulations of liquid silica: Equation of state and liquid-liquid phase transition. *Phys. Rev. E*, 63:011202, 2000.
- [47] Mahoney, M. W. & Jorgensen, W.L. A five-site model for liquid water and the reproduction of the density anomaly by rigid, nonpolarizable potential functions. *J. Chem. Phys.*, 112:8910–8922, 2000.
- [48] Ruocco, G. & Sette, F. The history of the "fast sound" in liquid water. *Condensed Matter Physics*, 11: 29–46, 2008.
- [49] Sampoli, M., Ruocco, G. & Sette, F. Mixing of longitudinal and transverse dynamics in liquid water. *Phys. Rev. Lett.*, 79:1678–1681, 1997.
- [50] Krishnamurthy, S., Bansil, R. & Wiafe-Akinten, J. Low-frequency Raman spectrum of supercooled water. *J. Chem. Phys.*, 79:5863–5870, 1983.
- [51] Klug, D. D., Whalley, E., Svensson, E. C., Root, J. H. & Sears, V. F. Densities of vibrational states and heat capacities of crystalline and amorphous H_2O ice determined by neutron scattering. *Phys. Rev. B*, 44:841–844, 1991.
- [52] McIntosh, C., Toulouse J, & Tick, P. The Boson peak in alkali silicate glasses. *Journal of Non-Crystalline Solids*, 222:335–341, 1997.
- [53] Novikov, V. N., Duval, E., Kisliuk, A. & Sokolov, A. P. A model of low frequency Raman scattering in glasses: Comparison of Brillouin and Raman data. *J. Chem. Phys.*, 102:4691–4698, 1995.
- [54] Bell, R. J., Dean, P. & Hibbins-Butler, D. C. The vibrational spectra of vitreous silica, germania and beryllium fluoride. *J. Phys. C: Solid State Physics*, 3:2111–2118, 1970.

- [55] Sastry, S., Stanley, H. E. & Sciortino, F. Low frequency depolarized Raman spectra in water: Results from normal mode analysis. *J. Chem. Phys.*, 100:5361–5366, 1994.
- [56] Shintani, H. & Tanaka, H. Universal link between the boson peak and transverse phonons in glass. *Nature Mat*, 7:870–877, 2008.
- [57] Matharoo, G. S., Shajahan, M., Razul, G. & Poole, P. H. Spectral statistics of the quenched normal modes of a network-forming molecular liquid . *J. Chem. Phys.*, 130:124512, 2009.

Acknowledgments

We thank S. V. Buldyrev and S. Sastry for helpful discussions. The simulations were in part performed using resources provided by the Swedish National Infrastructure for Computing (SNIC) at the NSC and HPC2N centers. LGMP, KTW and DS were supported by the Swedish Research Council. KTW is also supported by the Icelandic Research Fund through the START programme. PK acknowledges the support of National Academies Keck Future Initiatives award. HES thanks NSF Grants No. CHE0911389, No. CHE0908218, and No. CHE-1213217.

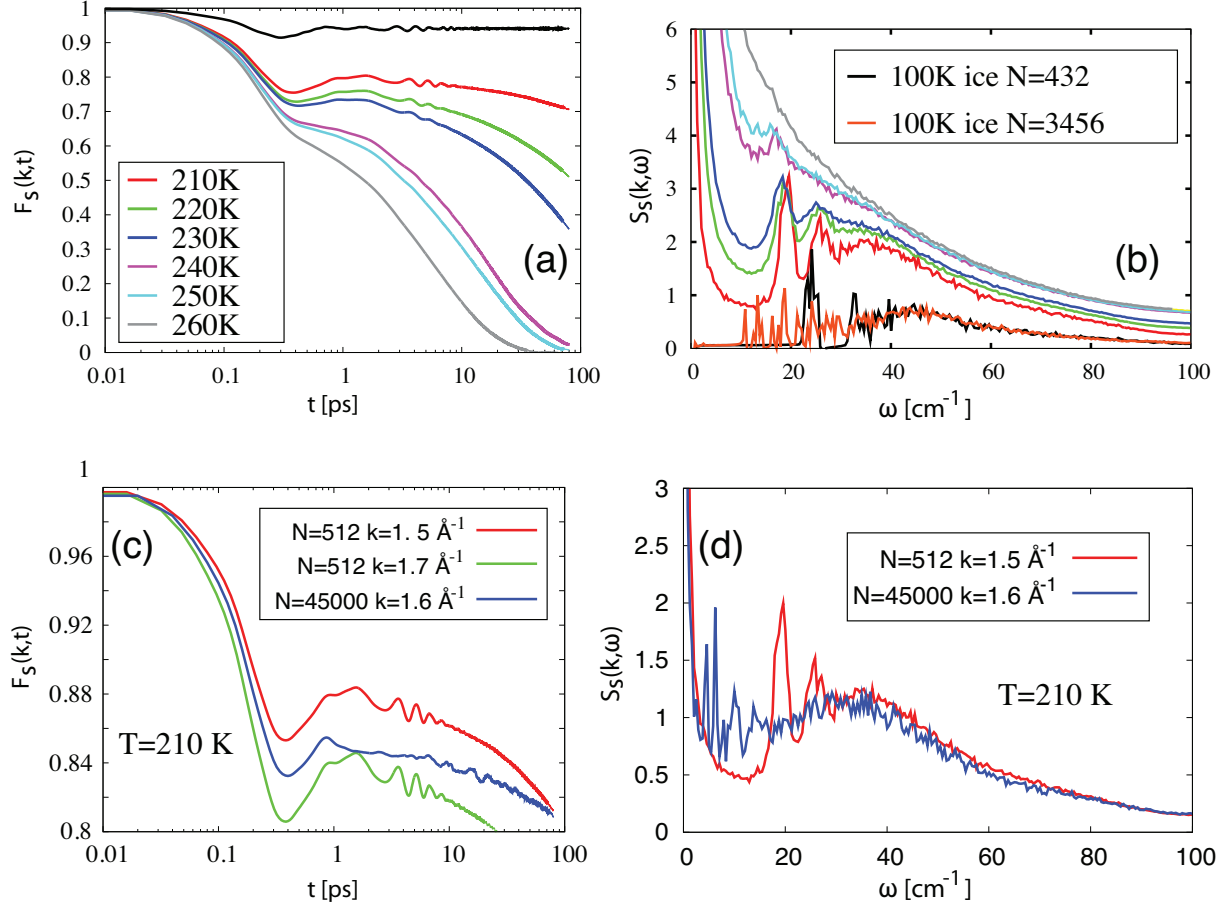


FIG. 1: (a) $F_s(k, t)$ and (b) $S_s(k, \omega)$ for a range of temperatures 210-260 K at fixed $k = 2.0 \text{ \AA}^{-1}$ and system size $N = 512$. $S_S(k, \omega)$ at $k = 2.0 \text{ \AA}^{-1}$ for ice at 100 K is also shown for two different system sizes, $N = 432$ and $N = 3456$. (c)-(d) show a comparison with $F_s(k, t)$ and $S_S(k, \omega)$ for a large $N = 45,000$ simulation at 210 K at $k \approx 1.6 \text{ \AA}^{-1}$. The broad peak around $\omega = 37 \text{ cm}^{-1}$ is evidently independent of system size while the sharper peaks at lower frequency are not present in the large simulation.

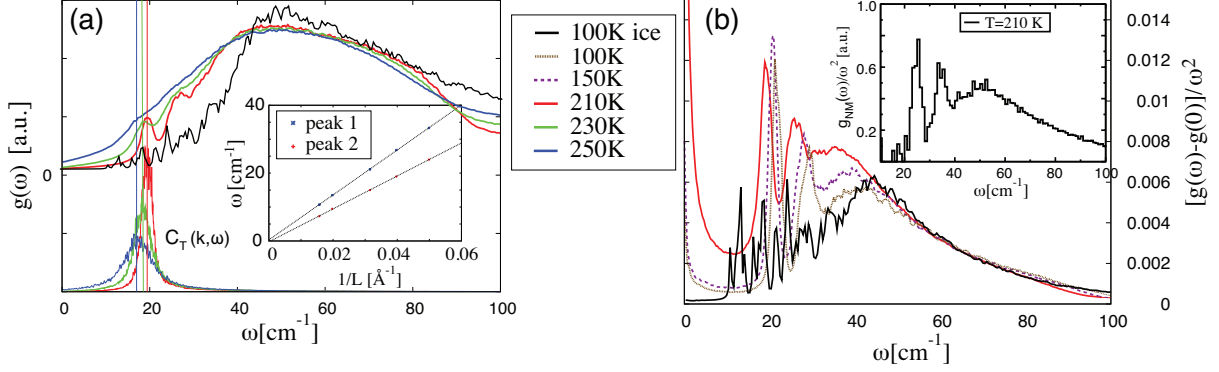


FIG. 2: Simulations of TIP4P/2005 water with $N = 512$. (a) VDOS of liquid water at supercooled temperatures and of hexagonal ice and (inset) inverse box-length dependence of the two lowest sharp peaks of the VDOS, extrapolating to zero frequency in the limit of infinite system size. In (a) the lowest- k transverse current spectrum is shown in the bottom part, illustrating that the sharp low-frequency peaks are low- k transverse modes. (b) Reduced vibrational density of states at low T calculated as $[g(\omega) - g(0)]/\omega^2$ with an extrapolated $g(0)$ to eliminate uncertainties related to the finite simulation time. Upon rapid cooling into a non-equilibrated LDA ice at 150 K and 100 K, the Boson peak is seen to shift to higher frequencies, approaching that of hexagonal ice. The inset in (b) shows the reduced VDOS calculated from the normal modes of inherent structures quenched from equilibrated $T=210$ K configurations. The normal mode $g_{NM}(\omega)/\omega^2$ shows a Boson peak which is blue-shifted to about the same frequency as the crystal, suggesting that as the liquid structure is made harmonic the Boson peak frequency shifts to higher values saturating at about 50 cm^{-1} .

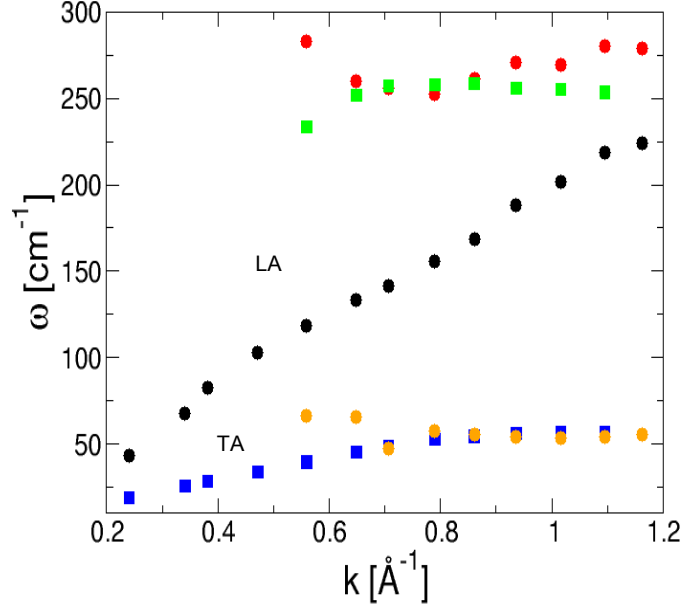


FIG. 3: Longitudinal (filled circles) and transverse (filled squares) dispersion relations calculated from the peak positions of $\omega_L(k)$ in $C_L(k, \omega)$ and $\omega_T(k)$ in $C_T(k, \omega)$ for $N=2048$ and $T=210\text{K}$. For $k < 0.5 \text{ \AA}^{-1}$, longitudinal spectra exhibit one dispersive branch (LA: black filled circles), while for $k > 0.5 \text{ \AA}^{-1}$, the longitudinal spectra exhibit three excitations –low and high frequency non-dispersive excitations (shown in orange and red filled circles). For $k < 0.5 \text{ \AA}^{-1}$ transverse current spectra exhibit only one dispersive excitation (TA: blue filled squares) while for $k > 0.5 \text{ \AA}^{-1}$, it exhibits both the dispersive branch as well as a non-dispersive excitation (green filled squares) at $\omega \approx 260 \text{ cm}^{-1}$. For information on extraction of the dispersion relation see Fig. S2.

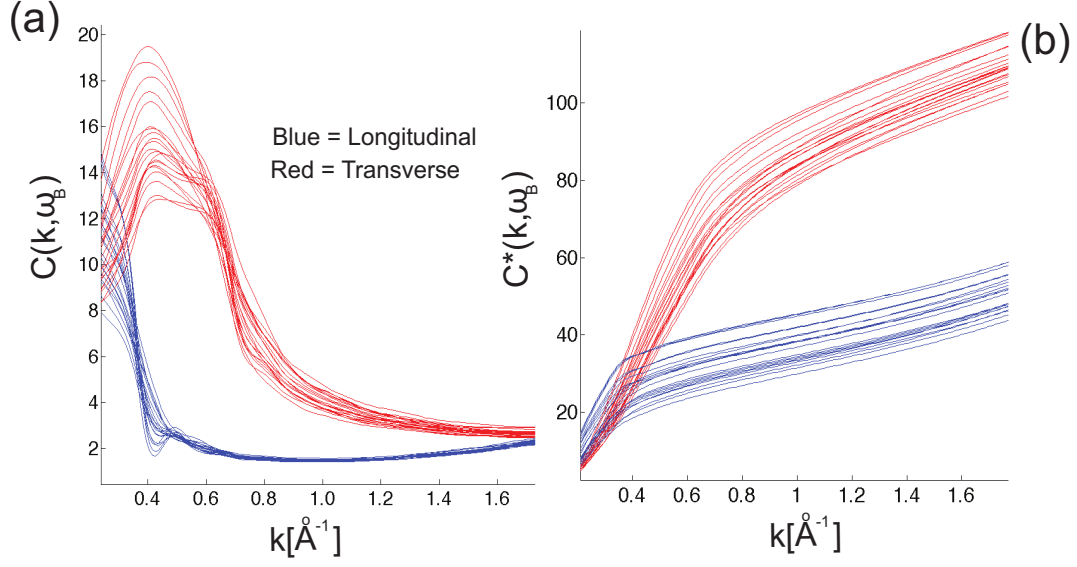


FIG. 4: (a) Current correlation functions $C_L(k, \omega_B)$ and $C_T(k, \omega_B)$ as function of k . (b) Integrated current correlation functions $C_L^*(k, \omega_B)$ and $C_T^*(k, \omega_B)$ as function of k (see Eq. 8). Several frequencies ω_B in the Boson peak frequency regime are shown.

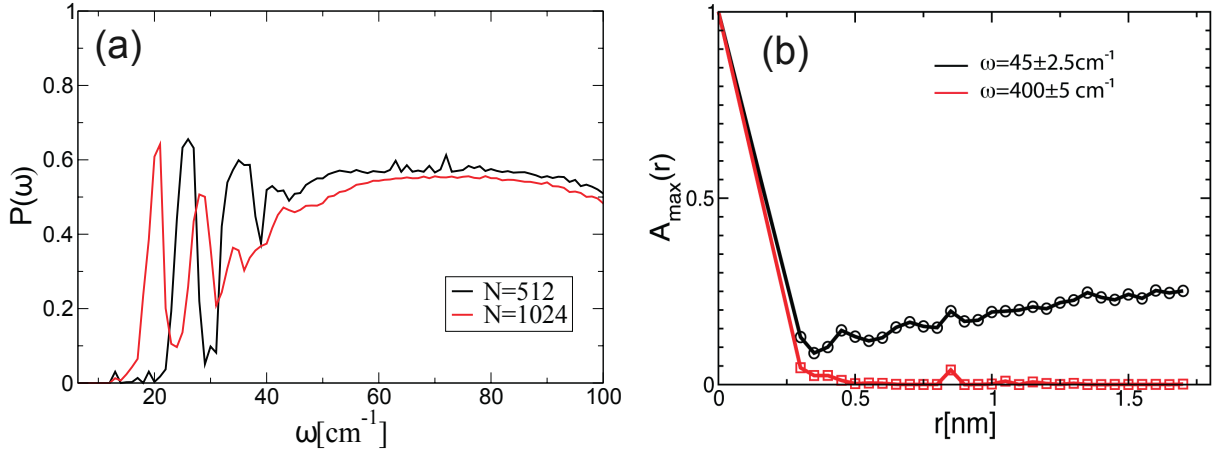


FIG. 5: (a) Frequency dependent participation ratio for two system sizes, $N = 512$ and $N = 1024$. (b) Spatial dependence of the amplitude of normal modes $A_{\max}(r)$ in the Boson peak regime. For a comparison, $A_{\max}(r)$ for $\omega = 400 \pm 5 \text{ cm}^{-1}$ where the modes are localized is also shown. The value of $A_{\max}(0)$ is normalized to 1 for the range of frequencies shown.

SUPPLEMENTARY INFORMATION

In Fig. S1 we show the self-intermediate scattering function $F_s(k, t)$ and the incoherent dynamic structure factor $S_s(k, \omega)$ of the TIP5P water model which differs significantly from the TIP4P/2005 model in terms of physical properties. The Widom line in this model is close to 250 K, which is also where the Boson peak in the model emerges.

In Fig. S2 we show the transverse and longitudinal current spectra $C_T(k, \omega)$ and $C_L(k, \omega)$ for TIP4P/2005 at $T=210$ K for small, intermediate, and large wave numbers.

In Fig. S3 we show a snapshot of an energy-minimized configuration taken from a simulation at $T = 210$ K. Molecules contributing the most to a given normal mode near the peak frequency of the Boson peak are highlighted. Specifically, we looked at the molecules whose displacement is larger than a certain percentage of the largest molecular displacement observed for the given normal mode. We find no significant localization indicating that the Boson peak corresponds to rather long-range collective motion in the system.

Figure S4 shows movies of normal modes associated with the first two sharp peaks in (a) and (b) respectively, and the Boson peak in (c).

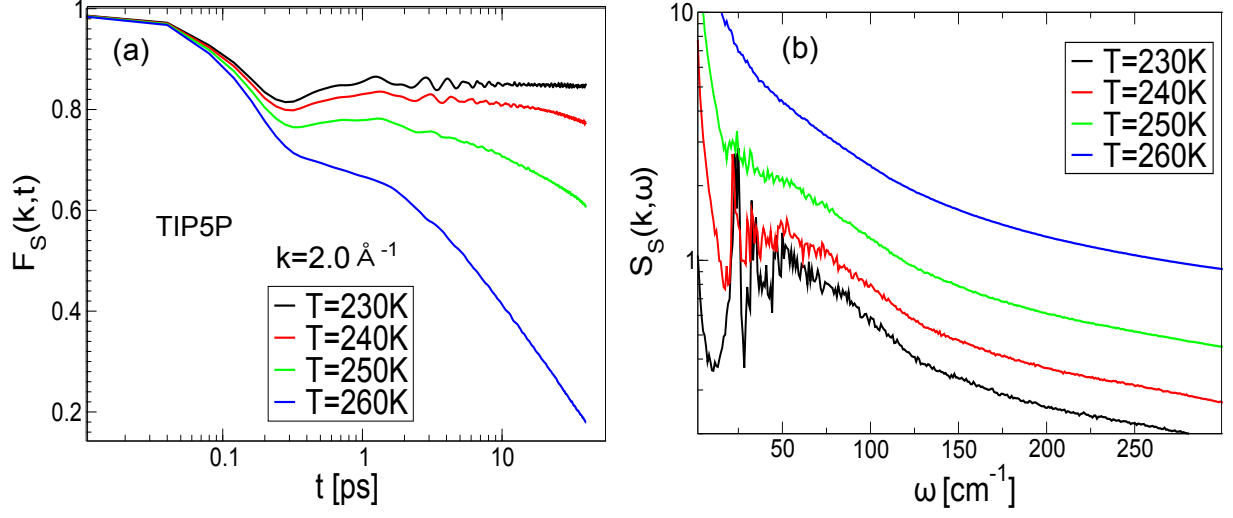


FIG. S1: (color online) (a) $F_s(k, t)$ and (b) $S_s(k, \omega)$ for temperatures between 230 and 260 K at $k \approx 2.0 \text{ \AA}^{-1}$ and system size $N = 512$ for the TIP5P water model. Below the Widom line temperature of the model, 250 K, a Boson peak around 50 cm^{-1} is seen to emerge.

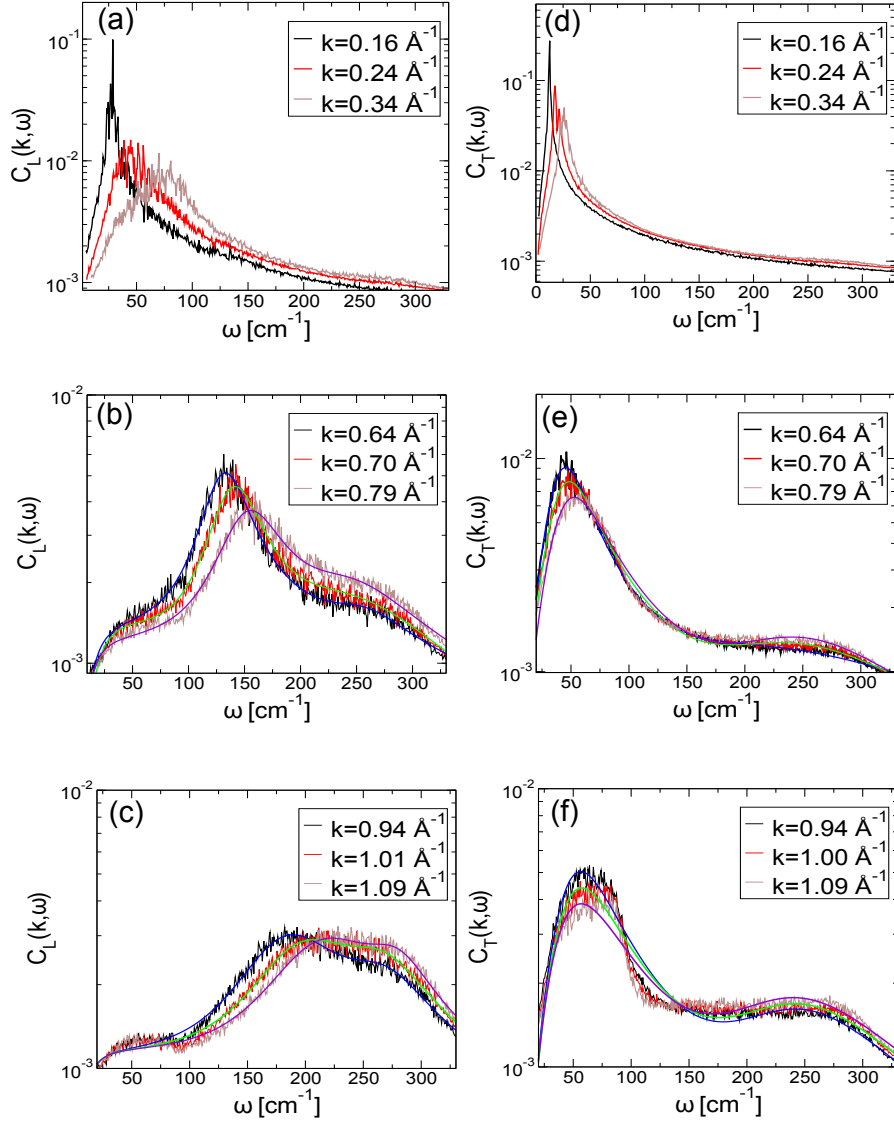


FIG. S2: (color online) Longitudinal current spectra $C_L(k, \omega)$ at $T=210$ K for (a) small, (b) intermediate, and (c) large wave numbers. Besides the dispersing peaks $C_L(k, \omega)$ develops two non-dispersive excitations –one at low frequency $\omega \approx 50 \text{ cm}^{-1}$ and a high-frequency excitation at about $\omega = 260 \text{ cm}^{-1}$ for $k > 0.5 \text{ \AA}^{-1}$ and the propagating branch tends to saturate to this frequency at large wave numbers. Transverse current spectra $C_T(k, \omega)$ for (d) small (e) intermediate, and (f) large wave numbers at $T=210$ K. For $k < 0.5 \text{ \AA}^{-1}$, $C_T(k, \omega)$ exhibits one dispersing excitation but for $k > 0.5 \text{ \AA}^{-1}$ two excitations are observed. DHO fits to the spectra for $k > 0.5 \text{ \AA}^{-1}$ are shown in solid lines. For $k > 0.5 \text{ \AA}^{-1}$, longitudinal spectra are fit with three DHO excitations while the transverse spectra are fit with two DHO excitations. Note that for $k > 0.5 \text{ \AA}^{-1}$, longitudinal spectra exhibit both low and high frequency excitations corresponding to transverse excitations.

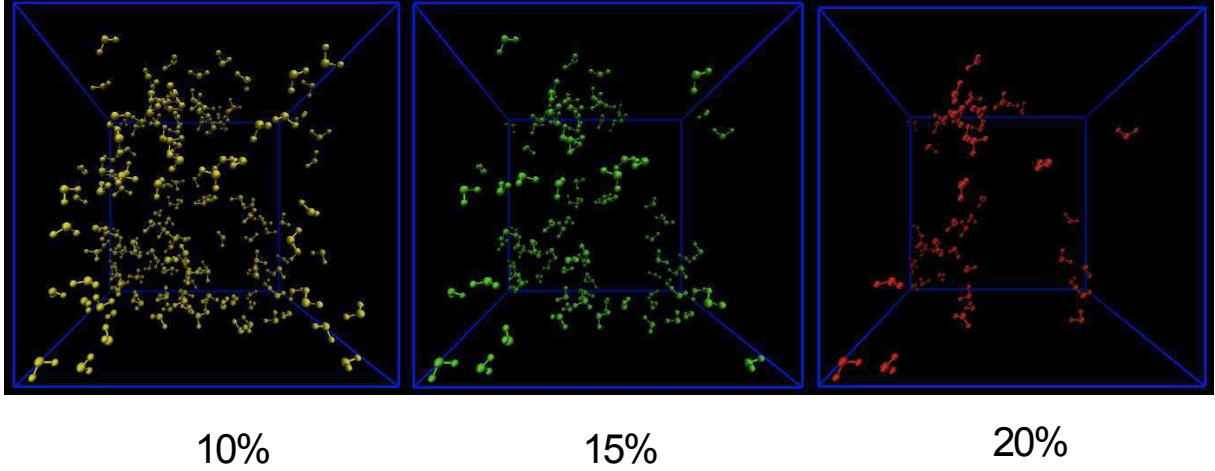


FIG. S3: (color online) Snapshot of a configuration showing the molecules involved in a representative eigenmode at the Boson peak. (a) The molecules colored yellow are those with displacements larger than 10% of the largest displacement of a molecule in the normal mode. (b) The molecules colored green are those with displacement larger than 15%, and (c) molecules with displacement larger than 20% are colored in red. We do not see significant localization in the low-frequency region where VDOS shows an excess.

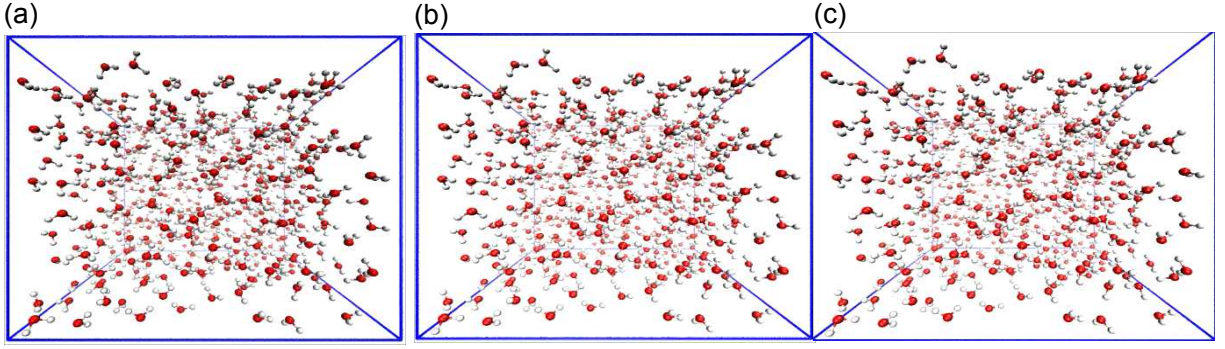


FIG. S4: Movies of normal modes corresponding to the first two spurious size-dependent peaks (a) , (b) and (c) the normal mode corresponding to the position of the Boson peak. Please refer to the included video files nmtrajFreq1.mpg, nmtrajFreq2.mpg, and nmtrajFreqBP.mpg respectively.